Wave Function Delocalization and Large-Amplitude Vibrations of Helium on Corrugated Aromatic Microsurfaces: Tetracene·He and Pentacene·He van der Waals Complexes†

Minzhong Xu and Zlatko Bačić*

Department of Chemistry, New York University, New York, New York 10003

Received: March 20, 2007; In Final Form: April 23, 2007

We report accurate quantum three-dimensional calculations of highly excited intermolecular vibrational states of the van der Waals (vdW) complexes tetracene·He and pentacene·He in the S_1 excited electronic state. The aromatic molecules were taken to be rigid and the intermolecular potential energy surfaces (IPESs) were modeled as a sum of atom−atom Lennard-Jones pair potentials. The IPESs are corrugated in the direction of the long (*x*) axis of the aromatic molecules, due to the presence of the symmetrically equivalent global double minimum for tetracene·He, and a triple minimum (central global minimum and two equivalent local minima) for pentacene·He, on each side of the aromatic plane. Both IPESs have two additional minor equivalent local minima further away from the center of the molecule. The vdW vibrational states analyzed in this work cover about 80% of the well depths of the IPESs. The mode coupling is generally weak for those states whose out-of-plane (*z*) mode is unexcited. However, the *z*-mode fundamental is strongly coupled to the short-axis (*y*) in-plane mode, so that the pure *z*-mode excitation could not be identified. The He atom exhibits large in-plane spatial delocalizaton already in the ground vdW vibrational state, which increases rapidly upon the excitation of the in-plane *x* and *y* modes, with little hindrance by the corrugation of the aromatic microsurfaces. For the vdW vibrational energies considered, the He atom spatial delocalization reaches Δx and Δy values of ∼5 and 4 Å, respectively, and is limited only by the finite size of the aromatic substrates. Side-crossing delocalization of the wave functions on both sides of the molecular plane is found at excitation energies >30 cm^{-1}, giving rise to the energy splittings of the pairs of states symmetric/antisymmetric with respect to the aromatic plane; the splittings show strong vdW vibrational mode specificity.

I. Introduction

Spectroscopy of large, planar aromatic molecules in helium has received a great deal of attention, experimental and theoretical, in recent years. Aromatic molecules such as anthracene, tetracene, and pentacene, with three, four, and five aromatic rings, respectively, can be viewed as nanoscale precursors to a bulk graphite surface, with the advantage that both their size and the nature of surface corrugation can be varied systematically. Experimental investigations of the electronic spectroscopy of helium-solvated large aromatic molecules can be divided into two broad classes: (i) those where the number of He atoms *n* is small ($n = 1-16$), and (ii) those involving an aromatic molecule embedded in a helium nanodroplet ($n = 10^3-10^4$). In the first category, for a small number of He atoms bound to naphthalene,[1] anthracene,[1,2] and tetracene,[1] the vibronic spectra of the $S_0 \rightarrow S_1$ transition exhibit discrete bands on the high-frequency side of the 0_0^0 transition, corresponding to the van der Waals (vdW) vibrational excitations in the S_1 excited electronic state. The number of bands reaches a maximum of 6, for tetracene solvated with 4 and 5 He atoms, and then surprisingly diminishes for larger clusters. In the combined experimental and theoretical study of the two-color resonant two-photon ionization (R2PI) spectra of the $S_0 \rightarrow S_1$ electronic transition of the 2,3-dimethylnaphthalene·He (2,3-DMN·He) vdW complex,[3] 5 bands were observed within 30 cm^{-1} of the electronic origin. On the basis of the quantum 3D bound-state calculations, 4 bands were assigned to intermolecular vibrational excitations, and the fifth to a vdW isomer.[3]

Electronic spectra of aromatic molecules inside helium nanodroplets exhibit some new features.[4] The 0_0^0 and other vibronic bands have sharp zero phonon lines (ZPL) followed by broader phonon wings on the blue side, arising from the collective compressional excitations of the helium droplet. The aromatic molecules whose $S_0 \rightarrow S_1$ electronic transitions inside helium nanodroplets have been studied include anthracene,[5] tetracene,[6−9] pentacene,[8,9] and phthalocyanines.[8,10] In the case of tetracene, the ZPL of the 0_0^0 band is split by 1.1 cm^{-1}, unlike the ZPL of pentacene, which is not split.[6−8] This splitting, whose origin is not clear, has been the subject of intense scrutiny. It has been tentatively attributed either to the occupation of two nearly equivalent sites by localized helium atoms or to a tunneling of one or two localized helium atoms, tightly bound to equivalent sites on the tetracene surface. But, a quantitative theory of the ZPL splitting in helium droplets remains to be developed.

On the theoretical side, highly excited large-amplitude vdW vibrational states, extensive wave function delocalization, strongly mode-specific side crossing and energy splittings in 2,3-DMN·He were studied using the quantum 3D DVR calculations.[3] These and other related issues were later investigated in depth for anthracene·He_n ($n = 1, 2$) vdW clusters by means of quantum mechanical calculations, under the approximation that anthracene is fixed in space, infinitely heavy.[11,12] Subsequently, a rigorous intermolecular vibrational Hamiltonian was derived for weakly bound complexes of this kind and applied to the

† Part of the "Roger E. Miller Memorial Issue".

* Author to whom correspondence should be addressed. Electronic mail: zlatko.bacic@nyu.edu.

10.1021/jp072218e CCC: $37.00
Published on Web 05/27/2007

quantum 6D calculation of the vdW vibrational levels of the (1|1) isomer of anthracene·He_2.[13] The ground-state energetics and structural aspects of the solvation by larger helium clusters have been studied with the help of quantum Monte Carlo methods for benzene−He_{39},[14] phthalocyanine·He_n ($n = 24-150$),[15] as well as anthracene·He_6 and tetracene·He_8.[16]

In this paper, we present the results of accurate quantum 3D calculations of highly excited vdW vibrational energy levels and wave functions of S_1 tetracene·He and pentacene·He vdW complexes. We believe that having a quantitative understanding of the intermolecular vibrational dynamics of a single He atom bound to tetracene and pentacene will be helpful in the development of a comprehensive theoretical treatment of the vibronic spectra of these molecules embedded in helium nanodroplets. Converged eigenstates are reported up to ~40 cm^{-1} above the vdW vibrational ground states of the complexes, covering about 80% of the well depths of the intermolecular potential energy surfaces (IPESs). Tetracene and pentacene are the largest linear aromatic molecules, i.e., provide the largest (linear) microsurfaces, for which the quantum dynamics of excited large-amplitude vibrations of the adsorbed He atom has been treated rigorously. In addition, tetracene and pentacene are the first members of the homologous series of linear polyacenes, for which the IPES of the binary complex with helium exhibit appreciable corrugation, in the form of multiple potential minima, along the long molecular axis. Consequently, tetracene·He and pentacene·He offer a unique opportunity for a rigorous study of the excited, exceptionally large-amplitude vibrations of the bound He atom, their level structure and mode coupling, as well as the very extensive spatial delocalization, and how they are affected by the surface corrugation. In addition, we explore the wave function delocalization by side crossing, which extends over both sides of the aromatic plane and gives rise to energy splittings; both are found to show strong vdW vibrational mode specificity.

II. Theory and Computational Aspects

A. Atom−Large Molecule Hamiltonian in the 3D DVR. The computational method employed in this work for the calculations of the 3D intermolecular vibrational ($J = 0$) levels of tetracene·He and pentacene·He was developed by Mandziuk and Bačić[17] and applied to a variety of vdW M·R complexes,[3,18−21] as well as the endohedral fullerene complex Ne@C_{70}.[22] Because a detailed description of the methodology is available,[17] only its key features are summarized here.

The frequencies of the intramolecular vibrational modes of the large molecule M are generally at least an order of magnitude higher than those of the intermolecular vibrations of the vdW M·R complexes. Hence M is taken to be rigid and the 3D subspace of the vdW vibrations of the complex is treated rigorously, as fully coupled. Following Brocks and van Koeven,[23] the intermolecular vibrations of M·R complexes are described in terms of three Cartesian components (x, y, z) of the vector connecting the center of mass of M and the atom R. The Cartesian axes are aligned with the principal axes of M, with x and y along the long and short in-plane axes of the aromatic molecule, respectively, and z perpendicular to the molecular plane. These coordinates are well suited for describing the motions of an atom bound to a highly anisotropic and corrugated microsurface of the planar substrate. Brocks and van Koeven have derived the vdW vibrational Hamiltonian in these M-fixed coordinates.[23]

All three intermolecular degrees of freedom the M·R complexes are treated in the discrete variable representation (DVR).[24,25] The versatility and the efficiency of the multidimensional DVRs have been demonstrated in demanding bound-state calculations arising in a wide range of problems, such as the size[26] and isomer[27] dependence of the vibrational frequency shifts in Ar_nHF clusters, the torsional levels of the water trimer[28−30] and tetramer,[31] vibrations of diatomic adsorbates on solid surfaces,[32] and the translation−rotation dynamics of hydrogen molecules inside the cages of the clathrate hydrates.[33,34] The DVR grid in several dimensions is readily tailored to the features of the PES and confined only to the physically relevant regions of the potential, those that are sampled by the wave functions at the excitation energies of interest. Moreover, it permits an effective implementation of the sequential diagonalization and truncation procedure,[24,25,35] capable of reducing drastically the size of the final Hamiltonian matrix without any loss of accuracy.

B. Symmetry-Adapted DVR Basis and Computational Parameters. The 3D DVR employed in this work and in our earlier calculations of M·R complexes is constructed as a direct product of 1D DVRs defined by 1D harmonic oscillator (HO) functions in x, y, and z, respectively, centered in the center of mass of the aromatic molecule M, tetracene, or pentacene. The feasible permutation-inversion (PI) symmetry group of both tetracene·He and pentacene·He is D_{2h}. As discussed at length previously,[17] the 3D DVRs symmetry adapted the irreducible representations (IRs) of this group are formed as a direct product of 1D DVRs, one for each of the three Cartesian coordinates, which have the required parity, even or odd. The parities of the 1D DVRs in x, y, and z coordinates, respectively, needed to form the 3D DVRs transforming under the different IRs of the D_{2h} symmetry group are given in Table 1 of ref 17.

Tetracene and pentacene are large molecules, shown in Figure 1, especially in the direction of the long (x) axis. Due to the light mass of the He atom, and the relatively weak corrugation of the IPES discussed below, the vibrational motions of the rare-gas atom parallel to the plane of M attain very large amplitudes, reaching up to 5 Å. In addition to this extensive in-plane delocalization, the He atom can delocalize completely around the aromatic molecule as well, through the side-crossing vibrations. Consequently, 3D DVR grids of large spatial extent must be employed. For both tetracene·He and pentacene·He, the range of the DVR was $0.0 < x < 8.0$ Å, $0.0 < y < 6.0$ Å, and $0.0 < z < 6.0$ Å. The dimensions of the 1D DVRs in x, y, and z directions were $N_x = 32$, $N_y = 24$, and $N_z = 60$, respectively. Hence, the size the direct-product 3D DVR basis is large, $N_x \times N_y \times N_z = 46\,080$. However, it was greatly reduced by means of the sequential diagonalization and truncation procedure. In the z coordinate, out of the $N_z = 60$ 1D (z mode) eigenstates obtained for each (x_α, y_β), only the $n_{cut}^{1D} = 10$ lowest-energy 1D eigenstates were retained for the next step. For the last step, $n_{cut}^{2D} = 30$ (35 for pentacene·He) lowest-energy 2D (yz) eigenstates, out of $N_y \times n_{cut}^{1D} = 240$, were kept at each DVR point x_α along the x axis. The dimension of the final Hamiltonian matrix, diagonalization of which yielded the 3D vdW vibrational eigenvalues and eigenvectors, was $N_x \times n_{cut}^{2D} = 960$ (1120 for pentacene·He), far smaller than that of the original direct-product 3D DVR basis, 46 080. Careful convergence tests have shown that with these basis set parameters the energy levels of interest, discussed in section III, are converged to better than 0.001 cm^{-1}.

The coordinates of the C and H atoms of tetracene and pentacene[36] are listed in Tables 1 and 2, respectively. The atomic masses (in amu) used in these calculations were He 4.0, C 12.0, and H 1.0.

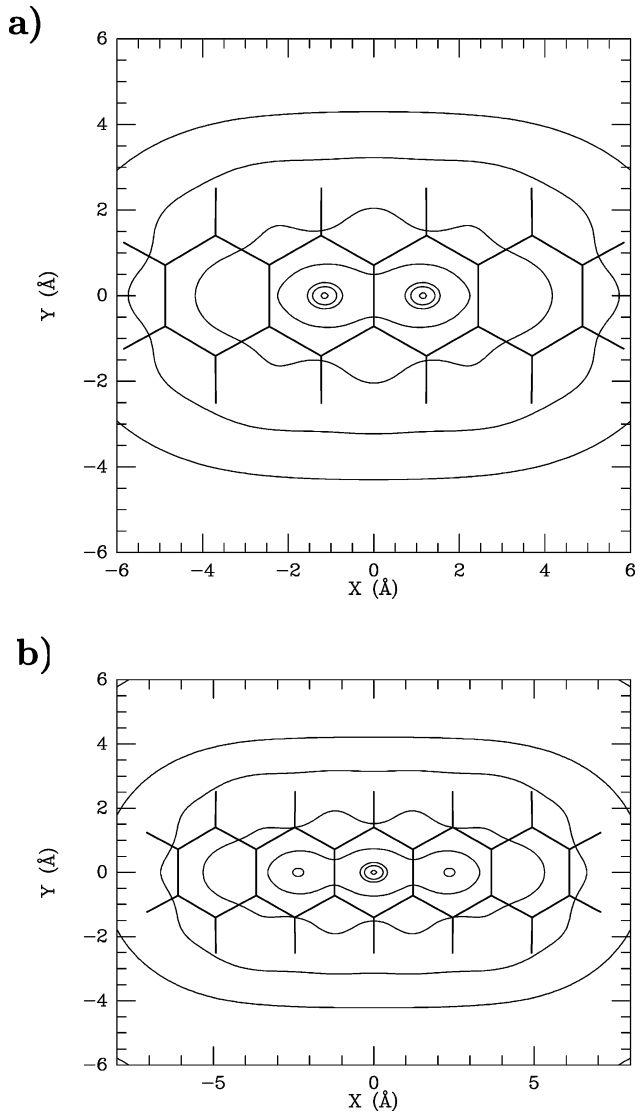

Figure 1. Contour plots of the intermolecular potential energy surfaces (IPESs) of tetracene·He (a) and pentacene·He (b), in the S_1 electronic state, for the parameters in Table 3. Potential cuts in the *xy* plane are shown for the *z* coordinate of the global minima of the two IPESs, $z = 3.096$ Å (a) and $z = 3.093$ Å (b), respectively. The first five contours are drawn at the energies of 0.1, 1, 2, 10, and 25 cm^{-1}, respectively, above the global minima of the IPESs. The energy spacing between the subsequent contours is 25 cm^{-1}.

C. Parametrization and Intermolecular Potential Energy Surfaces. As in our previous work on atom−large molecule complexes,[3,17−21] the IPESs of tetracene·He and pentacene·He in the S_1 state were represented as a sum over pairwise atom−atom 12−6 Lennard-Jones (LJ) potentials between the He atom and each C and H atom of tetracene or pentacene. The LJ parameters employed in this work are shown in Table 3; they are the product of an extensive optimization in ref 3, by minimizing the difference between the calculated vdW vibrational eigenstates and the four intermolecular vibrational excitations observed in the two-color R2PI spectra of the $S_0 \rightarrow S_1$ electronic transition of 2,3-DMN·He.

The resulting IPESs for S_1 tetracene·He and pentacene·He are shown in Figures 1 and 2. Particularly interesting are the 1D potential profiles along the *x* axis displayed in Figure 2. They reveal that tetracene·He has two symmetrically equivalent global minima on either side of the molecular plane, for the total of four, at (±1.151, 0.0, ±3.096 Å), with the calculated well depth $D_e = -100.84$ cm^{-1}. The barrier between the global minima is 6.5 cm^{-1} high, and they are flanked by two much shallower local minima that are ∼11 cm^{-1} higher in energy. For pentacene·He, on each side of the molecule there is the global minimum centrally located at (0.0, 0.0, ±3.093 Å) with $D_e = -102.91$ cm^{-1}, and two equivalent secondary minima at (±2.36, 0.0, ±3.095 Å) and $D_e = -101.30$ cm^{-1} ; the height of the barrier separating the global and the secondary minima is 7.8 cm^{-1}, relative to the global minimum. Further out in both directions on the *x* axis, as in tetracene·He, two minor equivalent local minima exist, ∼13 cm^{-1} above the global minimum.

Consequently, the two IPESs are corrugated in the direction of the long axis of the aromatic molecule. But, the corrugation of 11−13 cm^{-1}, small in comparison to the well depths of 100−103 cm^{-1}, is rather weak. Its effects on the vdW vibrational level structure and wave function delocalization are discussed below.

TABLE 1: Coordinates (Å) of C and H Atoms of Tetracene, Relative to the Center of Mass of the Molecule[a]

atom	*x*	*y*
C1	−1.233	1.404
C2	0.000	0.715
C3	1.233	1.404
C4	2.439	0.718
C5	3.702	1.406
C6	4.874	0.715
C7	4.874	−0.715
C8	3.702	−1.406
C9	2.439	−0.718
C10	1.233	−1.404
C11	0.000	−0.715
C12	−1.233	−1.404
C13	−2.439	−0.718
C14	−3.702	−1.406
C15	−4.874	−0.715
C16	−4.874	0.715
C17	−3.702	1.406
C18	−2.439	0.718
H1	−1.227	2.506
H2	1.227	2.506
H3	3.687	2.507
H4	5.842	1.238
H5	5.842	−1.238
H6	3.687	−2.507
H7	1.227	−2.506
H8	−1.227	−2.506
H9	−3.687	−2.507
H10	−5.842	−1.238
H11	−5.842	1.238
H12	−3.687	2.507

[a] The *z* cordinate is equal to zero for all atoms, because the molecule is planar.

III. Results and Discussion

The vdW vibrational levels calculated with the 3D DVR method are given in Table 4 for S_1 tetracene·He and in Table 5 for S_1 pentacene·He. The levels in both tables are labeled with two IRs of the D_{2h} symmetry group. The reason for this is that every level shown actually consists of a pair of nearly degenerate states which are symmetric and antisymmetric, respectively, with respect to the molecular plane. For excitation energies up to $\Delta E \approx 28$ cm^{-1} above the vibrational ground state, their wave functions are localized above and below the molecular plane, so that the energy splittings of the symmetric/antisymmetric pairs of states are very small, <0.001 cm^{-1}, below the numerical precision of our results. At higher energies, side-crossing wave function delocalization around the molecule takes place, resulting in increased energy splittings. When they

TABLE 2: Coordinates (Å) of C and H Atoms of Pentacene, Relative to the Center of Mass of the Molecule[a]

atom	*x*	*y*
C1	0.000	1.404
C2	1.220	0.717
C3	2.463	1.406
C4	3.662	0.721
C5	4.929	1.407
C6	6.099	0.717
C7	6.099	−0.717
C8	4.929	−1.407
C9	3.662	−0.721
C10	2.463	−1.406
C11	1.220	−0.717
C12	0.000	−1.404
C13	−1.220	−0.717
C14	−2.463	−1.406
C15	−3.662	−0.721
C16	−4.929	−1.407
C17	−6.099	−0.717
C18	−6.099	0.717
C19	−4.929	1.407
C20	−3.662	0.721
C21	−2.463	1.406
C22	−1.220	0.717
H1	0.000	2.505
H2	2.454	2.507
H3	4.914	2.508
H4	7.068	1.237
H5	7.068	−1.237
H6	4.914	−2.508
H7	2.454	−2.507
H8	0.000	−2.505
H9	−2.454	−2.507
H10	−4.914	−2.508
H11	−7.068	−1.237
H12	−7.068	1.237
H13	−4.914	2.508
H14	−2.454	2.507

[a] The *z* cordinate is equal to zero for all atoms, because the molecule is planar.

TABLE 3: Lennard-Jones Atom−Atom Potential Parameters σ and ϵ for the First Excited Electronic State (S_1) of Tetracene·He and Pentacene·He, Used in this Work (from Ref 3)

interaction	σ (Å)	ϵ (cm^{-1})
He−C	3.100	10.260
He−H	2.660	4.239

are ≥ 0.001 cm^{-1}, the energy splittings Δ are given in Tables 4 and 5. In addition, the root-mean-square (rms) amplitudes of the vdW vibrations, Δx, Δy, and Δz, along each of the Cartesian axes are shown. They provide a measure of the floppiness of the complexes in each vibrational state and are most helpful in making the quantum number assignments. The expected values of the Cartesian coordinates $\langle x \rangle$ and $\langle y \rangle$ are zero by symmetry. In principle, $\langle z \rangle = 0$ also; however, to characterize the *z* location of the wave function relative to the molecular plane, we define $\langle z \rangle$ over the *positive z* range only, which is given in Tables 4 and 5. Finally, Tables 4 and 5 include the approximate Cartesian quantum number assignments (υ_x, υ_y, υ_z), made with the help of Δx, Δy, and Δz values, nodal properties of the wave functions, and energy considerations.

The vdW vibrational ground-state energy of tetracene·He is −61.46 cm^{-1}, and that of pentacene·He is −63.24 cm^{-1}. Because the global minima of the two vdW complexes are at −100.84 and −102.91 cm^{-1}, respectively, their vdW vibrational zero-point energies (ZPEs), 39.39 cm^{-1} for tetracene·He and 39.67 cm^{-1} for pentacene·He, take up a significant fraction of the well depth, ∼39%. For comparison, in S_1 anthracene·He,

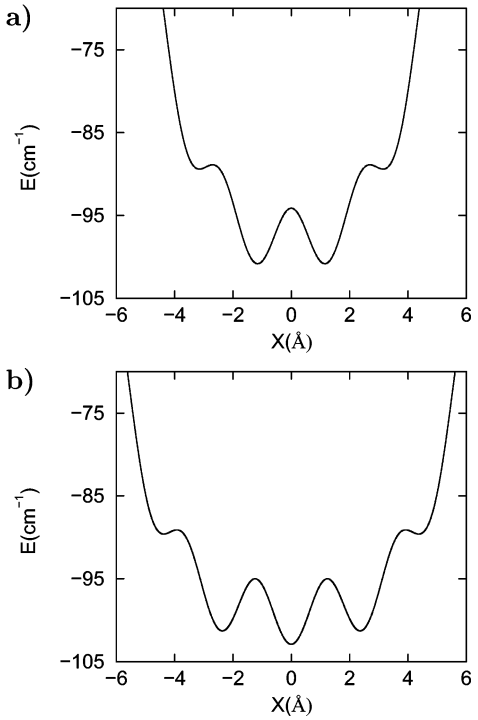

Figure 2. Intermolecular potential energy surfaces of tetracene·He (a) and pentacene·He (b), in the S_1 electronic state, as a function of *x*, for $y = 0.0$ Å and $z = 3.096$ Å (a) and $z = 3.093$ Å (b), respectively.

using a somewhat different parametrization of the IPES, the calculated ZPE[12] represents ∼34 % of the well depth.

The vdW vibrational states of tetracene·He in Table 4 extend to ∼19 cm^{-1} below the dissociation limit and cover ∼81% of the well depth of the IPES. For pentacene·He, the states in Table 5 come to within ∼25 cm^{-1} of the dissociation limit, covering ∼76 % of the well depth.

A. van der Waals Vibrational Mode Progressions and Mode Coupling. We first take a closer look at the states of tetracene·He and pentacene·He corresponding to the pure *x*-mode or *y*-mode excitations, (υ_x, 0, 0) and (0, υ_y, 0), respectively. Cuts through the wave functions representative of this category are shown in Figures 3−5. The regular nodal patterns evident in these cuts are indicative of generally weak vdW mode coupling for such states; a couple of exceptions are discussed below. States (υ_x, 0, 0) up to $\upsilon_x = 10$ for tetracene·He and $\upsilon_x = 11$ for pentacene·He, as well as (0, υ_y, 0) states up to 7 quanta in *y* for tetracene·He and up to 6 quanta in *y* for pentacene·He, were indentified; cf. Tables 4 and 5. Their energies are plotted as a function of υ_x and υ_y in Figures 6a,b, respectively. These plots show a remarkably even separation of the neighboring states belonging to the progressions (υ_x, 0, 0) and (0, υ_y, 0) over a wide range of quantum numbers. The spacing between the neighboring *x*-mode states is 4−5 cm^{-1} for tetracene·He, and ∼4 cm^{-1} for pentacene·He; the neighboring *y*-mode states are separated by ∼5 cm^{-1} in both complexes.

In the *x*-mode progression, the only states that deviate from this regularity are the low-lying ones. The two lowest-energy *x*-mode excitations of tetracene·He are at 3.27 and 8.16 cm^{-1}, and for pentacene·He they are at 2.37 and 4.77 cm^{-1}. The level spacings are uneven for states up to $\upsilon_x = 3$ and 4, for tetracene·He and pentacene·He, respectively, whose excitation energies ΔE are below 12 cm^{-1}. This is easily understood in terms of the corrugation of the IPES along the *x* axis, discussed at the end of section IIC. This weak corrugation of 11−13 cm^{-1} perturbs the *x*-mode states in the low-energy range, but not the

TABLE 4: Properties of the van der Waals Vibrational Levels of Tetracene·He in the First Excited Electronic State (S_1), Calculated Using the 3D DVR Method[a]

ΔE	Δx	Δy	$\langle z \rangle$	Δz	Δ	symmetry	(υ_x, υ_y, υ_z)
0.000	1.14	0.66	3.37	0.32		A_g, B_{1u}	(0, 0, 0)
3.271	1.75	0.65	3.37	0.32		B_{3u}, B_{2g}	(1, 0, 0)
8.158	2.33	0.69	3.40	0.32		A_g, B_{1u}	(2, 0, 0)
11.266	1.12	1.33	3.39	0.33		B_{2u}, B_{3g}	(0, 1, 0)
11.645	2.75	0.67	3.39	0.32		B_{3u}, B_{2g}	(3, 0, 0)
14.739	1.89	1.33	3.39	0.33		B_{1g}, A_u	(1, 1, 0)
16.065	2.82	0.72	3.39	0.33		A_g, B_{1u}	(4, 0, 0)
18.377	1.22	1.95	3.32	0.37		A_g, B_{1u}	(0, 2, 0)
18.480	2.33	1.39	3.39	0.34		B_{2u}, B_{3g}	(2, 1, 0)
21.041	3.02	0.87	3.40	0.34		B_{3u}, B_{2g}	(5, 0, 0)
21.954	2.08	1.90	3.34	0.37		B_{3u}, B_{2g}	(1, 2, 0)
22.681	2.63	1.37	3.40	0.34		B_{1g}, A_u	(3, 1, 0)
23.844	1.14	2.50	3.18	0.41		B_{2u}, B_{3g}	(0, 3, 0)
24.986	2.33	2.03	3.30	0.38		A_g, B_{1u}	(2, 2, 0)
26.125	3.39	0.82	3.42	0.35		A_g, B_{1u}	(6, 0, 0)
27.234	2.97	1.38	3.42	0.35		B_{2u}, B_{3g}	(4, 1, 0)
27.427	2.09	2.51	3.19	0.42		B_{1g}, A_u	(1, 3, 0)
28.811	1.19	2.88	3.04	0.50	0.001	A_g, B_{1u}	(0, 4, 0)
29.612	2.62	2.02	3.33	0.39		B_{3u}, B_{2g}	(3, 2, 0)
30.216	2.34	2.58	3.15	0.43		B_{2u}, B_{3g}	(2, 3, 0)
30.837	3.81	0.82	3.43	0.36		B_{3u}, B_{2g}	(7, 0, 0)
31.605	3.36	1.44	3.42	0.36		B_{1g}, A_u	(5, 1, 0)
32.370	2.15	2.88	3.06	0.51	0.002	B_{3u}, B_{2g}	(1, 4, 0)
33.627	1.22	3.28	2.86	0.62	0.021	B_{2u}, B_{3g}	(0, 5, 0)
33.907	3.37	1.92	3.36	0.39		A_g, B_{1u}	(4, 2, 0)
34.880	3.00	2.50	3.15	0.53	0.002	A_g, B_{1u}	(2, 4, 0)?
35.114	2.54	2.60	3.18	0.46	0.002	B_{1g}, A_u	(3, 3, 0)
35.139	3.58	1.97	3.28	0.50		A_g, B_{1u}	(8, 0, 0)?
35.684	3.81	1.62	3.40	0.40		B_{2u}, B_{3g}	(6, 1, 0)
37.196	2.23	3.28	2.88	0.63	0.027	B_{1g}, A_u	(1, 5, 0)
37.282	1.58	2.51	3.36	0.96	0.073	A_g, B_{1u}	(0, 0, 1)?
37.565	3.93	2.01	3.32	0.44	0.001	B_{3u}, B_{2g}	(5, 2, 0)
38.460	1.23	3.01	3.10	1.08	0.144	A_g, B_{1u}	(0, 6, 0)?
38.856	4.63	1.29	3.37	0.41		B_{3u}, B_{2g}	(9, 0, 0)
39.218	4.30	1.83	3.33	0.45	0.002	B_{1g}, A_u	(7, 1, 0)
39.344	3.22	2.67	3.17	0.49	0.006	B_{2u}, B_{3g}	(4, 3, 0)
39.640	2.48	3.32	2.83	0.67	0.039	B_{2u}, B_{3g}	(2, 5, 0)
40.822	4.47	2.26	3.19	0.52	0.008	A_g, B_{1u}	(6, 2, 0)?
41.153	1.39	4.31	2.02	1.08	0.812	B_{2u}, B_{3g}	(0, 7, 0)?
41.956	5.19	1.35	3.28	0.48	0.003	A_g, B_{1u}	(10, 0, 0)

[a] The excitation energies ΔE (in cm^{-1}) are relative to the ground-state energy $E_0 = -61.458$ cm^{-1}. Δx, Δy, $\langle z \rangle$, and Δz are in Å. The energy splitting Δ (in cm^{-1}) of the pair of states which are symmetric or antisymmetric with respect to the molecular plane is shown only if ≥ 0.001 cm^{-1}; ΔE shown is that of the symmetric member of the pair. The levels are labeled by the irreducible representations of the D_{2h} symmetry group. Cartesian quantum number assignments (υ_x, υ_y, υ_z) are also given; those marked with ? are uncertain due to strong mode mixing.

TABLE 5: Properties of the van der Waals Vibrational Levels of Pentacene·He in the First Excited Electronic State (S_1), Calculated Using the 3D DVR Method[a]

ΔE	Δx	Δy	$\langle z \rangle$	Δz	Δ	symmetry	(υ_x, υ_y, υ_z)
0.000	1.34	0.65	3.37	0.31		A_g, B_{1u}	(0, 0, 0)
2.373	2.29	0.65	3.37	0.32		B_{3u}, B_{2g}	(1, 0, 0)
4.770	2.52	0.64	3.37	0.32		A_g, B_{1u}	(2, 0, 0)
8.982	2.99	0.68	3.39	0.32		B_{3u}, B_{2g}	(3, 0, 0)
11.257	1.37	1.31	3.39	0.33		B_{2u}, B_{3g}	(0, 1, 0)
11.775	3.52	0.67	3.39	0.32		A_g, B_{1u}	(4, 0, 0)
13.559	2.23	1.32	3.39	0.33		A_u, B_{1g}	(1, 1, 0)
15.087	3.58	0.67	3.39	0.32		B_{3u}, B_{2g}	(5, 0, 0)
16.327	2.73	1.30	3.39	0.33		B_{2u}, B_{3g}	(2, 1, 0)
18.218	1.88	1.80	3.33	0.36		A_g, B_{1u}	(0, 2, 0)
19.171	3.47	0.98	3.38	0.33		A_g, B_{1u}	(6, 0, 0)?
19.287	3.08	1.37	3.39	0.34		B_{1g}, A_u	(3, 1, 0)
20.612	2.26	1.94	3.32	0.36		B_{3u}, B_{2g}	(1, 2, 0)
22.567	3.31	1.36	3.40	0.34		B_{2u}, B_{3g}	(4, 1, 0)
23.224	3.86	0.71	3.40	0.33		B_{3u}, B_{2g}	(7, 0, 0)
23.521	2.88	1.94	3.33	0.37		A_g, B_{1u}	(2, 2, 0)
23.903	1.47	2.47	3.19	0.41		B_{2u}, B_{3g}	(0, 3, 0)
25.697	2.86	2.08	3.27	0.40		B_{1g}, A_u	(1, 3, 0)?
25.843	3.15	2.02	3.31	0.38		B_{3u}, B_{2g}	(3, 2, 0)
26.605	3.08	1.92	3.32	0.39		B_{1g}, A_u	(5, 1, 0)?
27.389	4.10	0.89	3.40	0.35		A_g, B_{1u}	(8, 0, 0)
28.834	1.65	2.79	3.07	0.49		A_g, B_{1u}	(0, 4, 0)
29.073	3.03	2.49	3.20	0.41		B_{2u}, B_{3g}	(2, 3, 0)
29.525	3.19	2.02	3.32	0.38		A_g, B_{1u}	(4, 2, 0)
29.967	3.84	1.38	3.41	0.35		B_{2u}, B_{3g}	(6, 1, 0)
30.843	2.33	2.82	3.06	0.49	0.001	B_{3u}, B_{2g}	(1, 4, 0)
31.017	3.19	2.55	3.16	0.43		B_{1g}, A_u	(3, 3, 0)?
31.517	4.53	0.88	3.42	0.36		B_{3u}, B_{2g}	(9, 0, 0)
33.333	3.56	2.01	3.34	0.39		B_{3u}, B_{2g}	(5, 2, 0)
33.632	1.46	3.23	2.88	0.60	0.014	B_{2u}, B_{3g}	(0, 5, 0)
33.651	4.22	1.44	3.42	0.36		B_{1g}, A_u	(7, 1, 0)
33.940	3.10	2.87	3.07	0.50	0.002	A_g, B_{1u}	(2, 4, 0)
34.990	3.14	2.53	3.19	0.43		B_{2u}, B_{3g}	(4, 3, 0)
35.169	4.89	1.00	3.42	0.39		A_g, B_{1u}	(10, 0, 0)
35.699	2.26	3.24	2.88	0.60	0.015	B_{1g}, A_u	(1, 5, 0)
35.734	3.22	2.93	3.02	0.51	0.002	B_{3u}, B_{2g}	(3, 4, 0)
36.668	3.38	2.08	3.36	0.52	0.005	A_g, B_{1u}	(6, 2, 0)
37.194	4.61	1.54	3.41	0.38		B_{2u}, B_{3g}	(8, 1, 0)
37.602	2.39	2.67	3.23	0.89	0.044	A_g, B_{1u}	(0, 0, 1)?
38.452	4.90	1.43	3.40	0.50	0.004	B_{3u}, B_{2g}	(11, 0, 0)?
38.633	1.52	2.67	3.29	1.02	0.082	A_g, B_{1u}	(0, 6, 0)?
38.665	3.79	2.55	3.21	0.44	0.002	B_{1g}, A_u	(5, 3, 0)
38.712	3.13	3.28	2.88	0.62	0.020	B_{2u}, B_{3g}	(2, 5, 0)

[a] The excitation energies ΔE (in cm^{-1}) are relative to the ground-state energy $E_0 = -63.236$ cm^{-1}. Δx, Δy, $\langle z \rangle$, and Δz are in Å. The energy splitting Δ (in cm^{-1}) of the pair of states which are symmetric or antisymmetric with respect to the molecular plane is shown only if ≥ 0.001 cm^{-1}; ΔE shown is that of the symmetric member of the pair. The levels are labeled by the irreducible representations of the D_{2h} symmetry group. Cartesian quantum number assignments (υ_x, υ_y, υ_z) are also given; those marked with ? are uncertain due to strong mode mixing.

states at higher energies, explaining the pattern of levels spacings observed in Figure 6a. It should be noted that this picture implies very weak coupling of the *x* mode to the vibrations in the *y* and *z* directions, which makes the ZPEs of the latter unavailable to the *x*-mode vibrations (the ZPE of which must be very small, certainly no more than 2 cm^{-1} out of the total ZPEs of 39−40 cm^{-1}).

The levels of the *y*-mode progression shown in Figure 6b, besides being evenly spaced, ~5 cm^{-1} apart for $\upsilon_y > 2$, have almost identical energies for tetracene·He and pentacene·He, unlike the states belonging to the *x*-mode progressions. This is perhaps not too surprising, because one expects the two vdW complexes to have very similar potentials governing the *y* motion of the He atom. But, this is also another manifestation of the weak coupling between *x* and *y* modes, as well as the *z* mode discussed below.

In addition to pure *x*- and *y*-mode states the majority, although not all, of combination states (υ_x, υ_y, 0), with simultaneous excitation in *x* and *y*, considered in this work have rather regular wave functions and are readily assignable; two typical examples are displayed in Figure 7. Plots of the energies of states (υ_x, 1, 0), (υ_x, 2, 0), and (υ_x, 3, 0) as function of υ_x, for tetracene·He and pentacene·He, are presented in Figure 8. They demonstrate clearly that the excitation energies of the *x* and *y* modes are very close to additive, confirming the weak coupling of these modes.

The vdW vibrational states discussed so far had no excitation of the *z* mode, perpendicular to the molecular plane. Identifying the state corresponding to fundamental *z*-mode excitation proved difficult for both complexes, due to the high level density and strong mode coupling in the energy range of 37−40 cm^{-1}, where the *z* fundamental is found in related vdW complexes.[3] In the case of tetracene·He, several considerations narrowed the choice

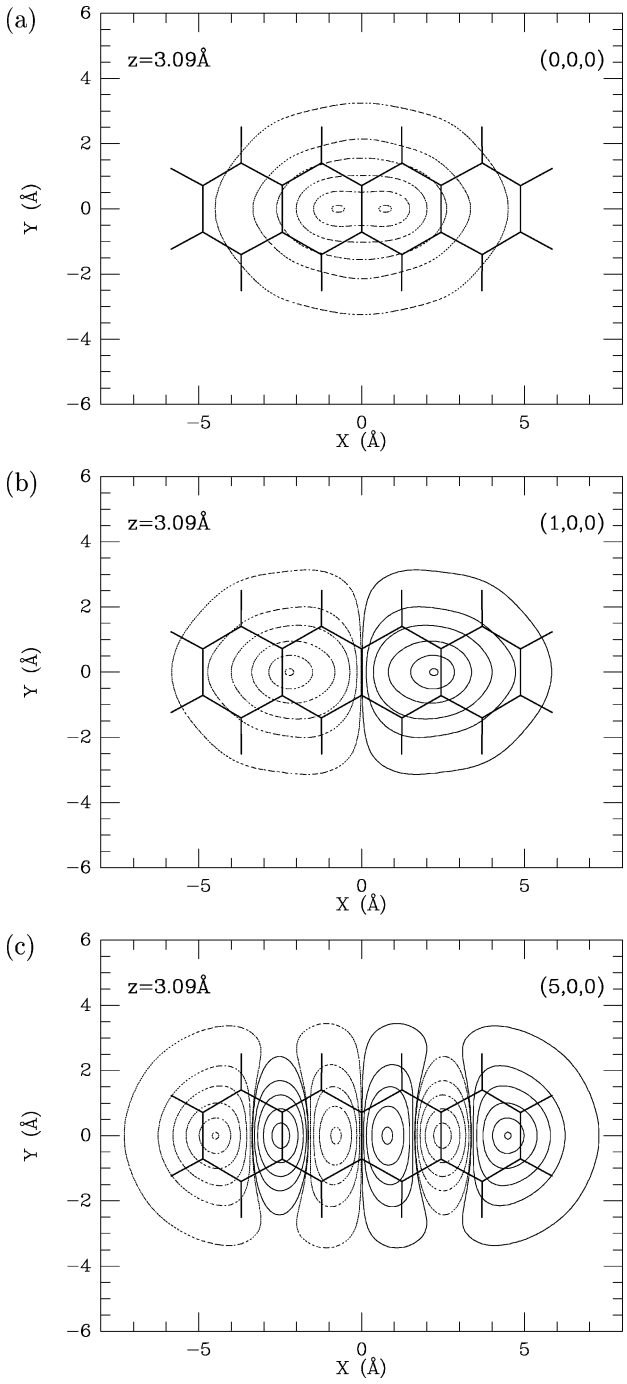

Figure 3. Cuts through the wave functions of three vdW states of tetracene·He, (0, 0, 0), (1, 0, 0), and (5, 0, 0). Contours are for 99, 80, 50, 25, 1, and 0.1% of the maximum amplitude for the respective cuts.

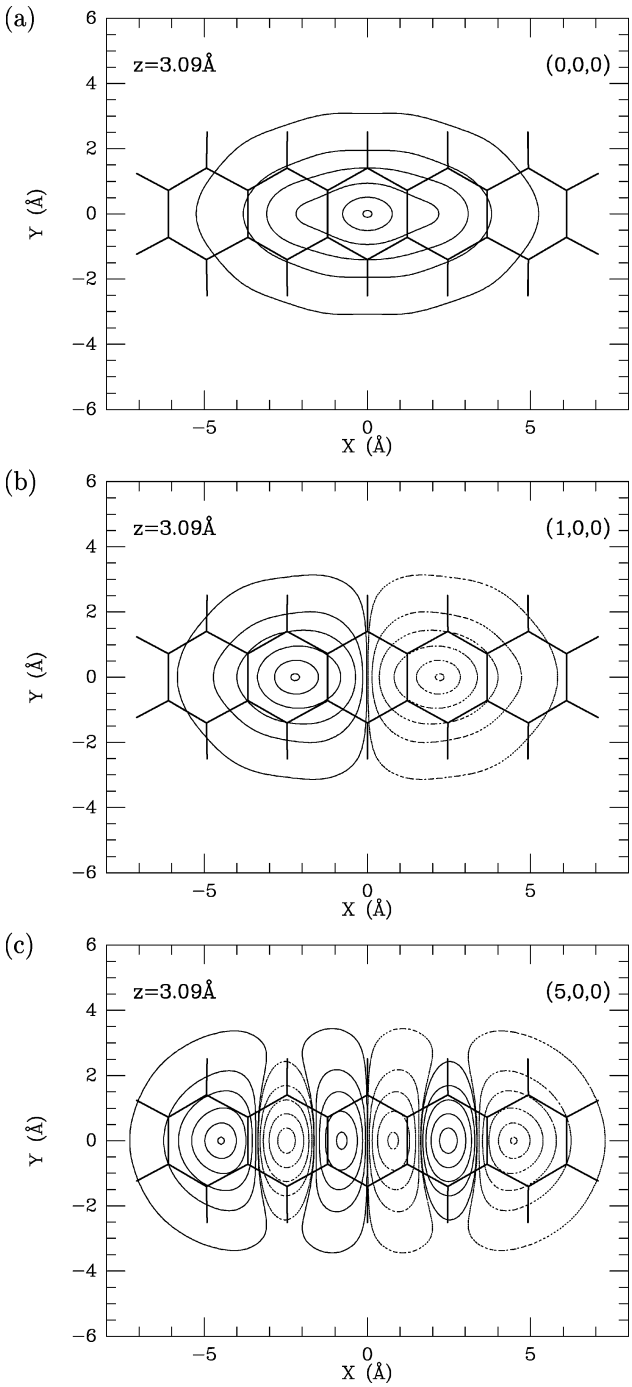

Figure 4. Cuts through the wave functions of three vdW states of pentacene·He, (0, 0, 0), (1, 0, 0), and (5, 0, 0). Contours are for 99, 80, 50, 25, 1, and 0.1% of the maximum amplitude for the respective cuts.

down to two states in Table 4, one at 37.282 cm^{-1} and the other at 38.460 cm^{-1}. They have the largest Δz values, 0.96 and 1.08 Å, respectively, of all the states up to these energies, and relatively small values of Δx. This indicates the excitation of the *z* mode, with the *x* mode in the ground state. However, both candidate states also have large Δy values, 2.51 and 3.01 Å, respectively, typical for states with *y*-mode excitation. Consequently, the *y* and *z* modes are very strongly mixed in the two states, making their assignment problematic. The assignment of the state at 37.282 cm^{-1} as (0, 0, 1)?, instead of the state at 38.460 cm^{-1}, rested on the following arguments: (i) it has the larger value of $\langle z \rangle$, (ii) the smaller value of Δy, and (iii) its energy splitting is a factor of 2 smaller than that of the other state. As discussed in section IIID, the magnitude of the energy splitting is linked to the degree of the *y*-mode excitation. This left the state at 38.460 cm^{-1} with (0, 6, 0)? assignment, based on the energy considerations (excellent fit in the *y*-mode progression), small Δx value, large value of Δy and of the energy splitting. We emphasize the tentative nature of both assignments, because of the unusually strong $y-z$-mode mixing.

Exactly the same problem was encountered in pentacene·He. Two states in Table 5, at 37.602 and 38.633 cm^{-1}, were identified as the candidates for the *z*-mode fundamental. Just as their counterparts in tetracene·He above, these two states exhibit all of the manifestations of very strong mixing of the *y* and *z* modes. They were assigned tentatively as (0, 0, 1)? and (0, 6, 0)?, respectively, following the reasoning used for

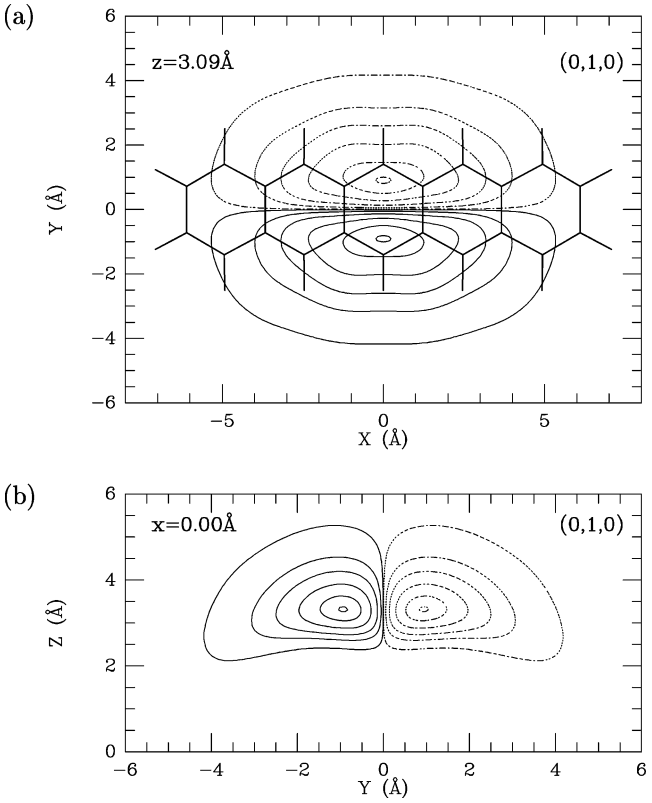

Figure 5. Cuts through the wave function of the vdW state (0, 1, 0) of pentacene·He in the *xy* (a) and the *yz* (b) planes. Contours are for 99, 80, 50, 25, 1, and 0.1% of the maximum amplitude for the respective cuts.

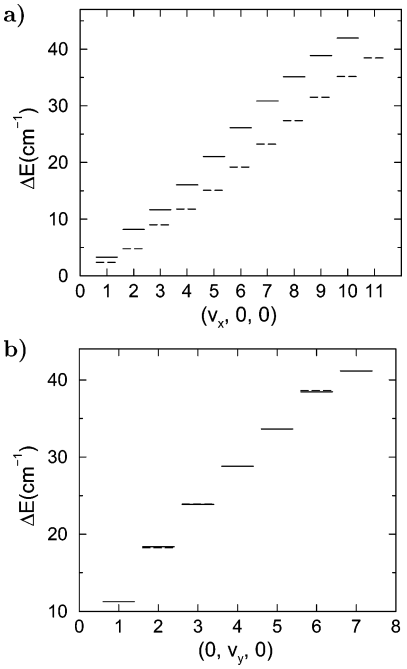

Figure 6. Excitation energies ΔE of the *x*-mode states (υ_x, 0, 0) vs υ_x (a) and the *y*-mode states (0, υ_y, 0) vs υ_y (b) of tetracene·He (full line) and pentacene·He (dashed line).

tetracene·He. One is led to conclude that on the IPES employed, neither tetracene·He nor pentacene·He has a state that represents a pure fundamental excitation of the *z* mode. For both complexes, the fundamental *z*-mode frequency is in the 37−39 cm^{-1} range, similar to the *z*-mode fundamental of 39.7 cm^{-1} calculated for 2,3-DMN·He.[3]

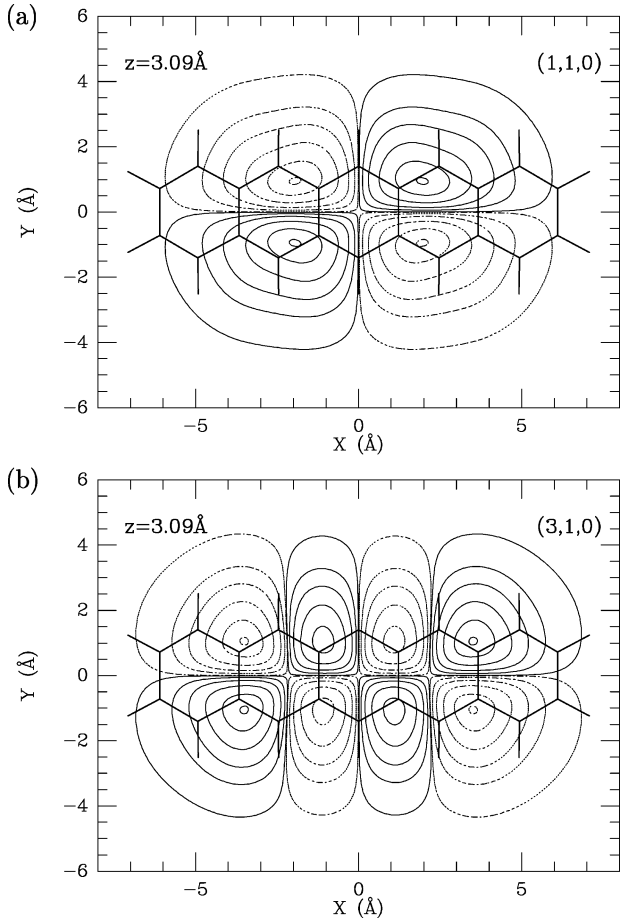

Figure 7. Cuts through the wave functions of two vdW states of pentacene·He, (1, 1, 0) and (3, 1, 0). Contours are for 99, 80, 50, 25, 1, and 0.1% of the maximum amplitude for the respective cuts.

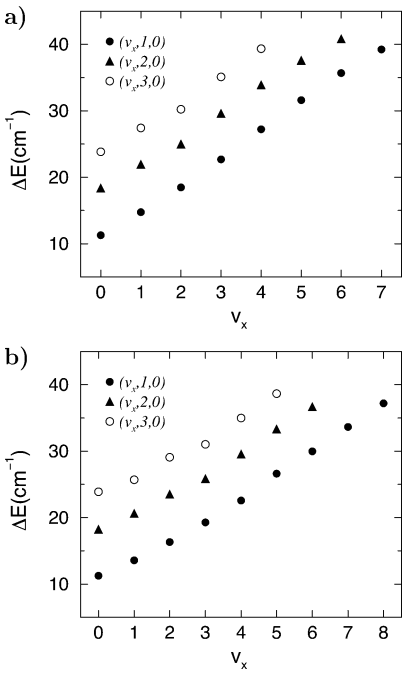

Figure 8. Excitation energies ΔE of states (υ_x, 1, 0), (υ_x, 2, 0), and (υ_x, 3, 0), as a function of υ_x, for tetracene·He (a) and pentacene·He (b).

B. Spatial Delocalization of van der Waals Vibrational States on Aromatic Microsurfaces. Characterizing the extent of spatial (de)localization of He atoms on finite aromatic

TABLE 6: Spatial Delocalization of the Ground van der Waals Vibrational States of Anthracene·He, Tetracene·He, and Pentacene·He in the S_1 Electronic State[a]

complex	Δx	Δy	Δz	$\langle z \rangle$
anthracene·He[b]	0.99	0.54	0.30	3.36
tetracene·He	1.14	0.66	0.32	3.37
pentacene·He	1.34	0.65	0.31	3.37

[a] Δx, Δy, Δz, and $\langle z \rangle$ are in Å. [b] Reference 11.

microsurfaces has been the subject of considerable theoretical effort. In the path-integral Monte Carlo (PIMC) calculations for the benzene$-He_{39}$ clusters over the temperature range 0.6−5 K, two helium atoms were found to be almost completely localized in the equivalent global minima of the IPES above and below the molecular plane, on the C_6 axis of benzene.[14] The classical-like spatial localization was attributed to the repulsive interaction between helium and the π-electron cloud of benzene, which creates a 6-fold barrier around the global minimum of the IPES. On the basis of this analysis, it has been proposed that strong lateral, in-plane confinement of individual He atoms on aromatic substrates is a general phenomenon and should occur also for larger planar aromatic molecules. e.g., naphthalene and tetracene.[14]

But, the subsequent quantum bound-state calculations of S_1 anthracene·He have shown significant wave function delocalization along the long (x) axis even in ground vdW vibrational state.[11,13] In Table 6, these results are combined with those obtained in this work for tetracene·He and pentacene·He. It is clear that in the ground vdW vibrational state, the spatial delocalization of the He atom parallel to the aromatic plane, measured by Δx, increases markedly with the size of the aromatic substrate, from 0.99 Å for anthracene·He, which has three linearly connected aromatic rings, to 1.34 Å for pentacene·He, with five linearly arranged aromatic rings. In contrast, the delocalization in the y and z directions is much smaller and hardly changes with the size of aromatic molecule, as expected for linear aromatics. The vibrationally averaged distance of the He atom to the aromatic plane is virtually the same for all three complexes, $\langle z \rangle = 3.36 - 3.37$ Å. We conclude that spatial localization of the He atom above (and below) the center of the aromatic ring is specific to benzene, due to its small size (single aromatic ring), and does not manifest in larger linear polyacenes, such as anthracene, tetracene, and pentacene.

The delocalization parallel to the aromatic microsurface increases rapidly with the excitation of the in-plane x and y vibrational modes, with little hindrance from the weak corrugation of the IPESs. Figure 9 shows that for the progressions (υ_x, 0, 0) and (0, υ_y, 0) of tetracene·He and pentacene·He, Δx and Δy grow strongly with increasing υ_x and υ_y, respectively, reaching up to ∼5 Å along the x axis and up to ∼4 Å in the y direction. The same range of Δx and Δy values was calculated for the vdW complex 2,3-DMN·He.[3] The rms amplitudes Δz are at least 2−3 times smaller for most states, indicating that the He atom moves much more freely parallel to the aromatic plane than in the direction perpendicular to it. At excitation energies of 35−40 cm^{-1}, the wave functions are spread over the entire microsurfaces of tetracene and pentacene; spatial delocalization of the He atom is essentially limited only by the finite size of the substrate molecule.

It is also evident from Figure 9 that the increase of Δx with υ_x, or Δy with υ_y, is not monotonic, and sometimes these rms amplitudes even *decrease* with increasing quantum number. This happens for states (8, 0, 0)? of tetracene·He and (6, 0, 0)? of pentacene·He, in Figure 9a. Inspection of Tables 4 and 5 shows that for both states Δy is significantly larger than for the other

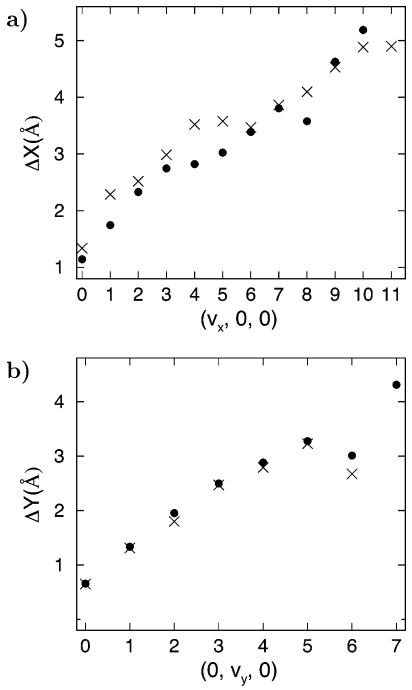

Figure 9. Root-mean-square amplitudes Δx for the x-mode states (υ_x, 0, 0) vs υ_x (a) and Δy for the y-mode states (0, υ_y, 0) vs υ_y (b), of tetracene·He (●) and pentacene·He (×).

members of their respective x-mode progressions, suggesting considerably stronger mixing with the y mode. Consequently, states (8, 0, 0)? and (6, 0, 0)? have less x-mode character, and this is reflected in comparatively smaller Δx values. Similarly, Figure 9b shows a pronounced dip in Δy for $\upsilon_y = 6$, for both tetracene·He and pentacene·He. Again, this is caused by mode mixing; as discussed earlier in section IIIA, for both vdW complexes in state (0, 6, 0)? the y mode is strongly mixed with the mode in z, resulting in smaller Δy. Interestingly, despite their strongly mixed character, states (8, 0, 0)? of tetracene·He and (6, 0, 0)? of pentacene·He, as well states (6, 0, 0)? of both complexes, fit very well their respective x- and y-mode progressions. Clearly, the level energies are much less sensitive to mode mixing than the wave function properties.

Finally, we point out a small discontinuity, or a plateau, visible in the plots of Δx vs υ_x in Figure 9a for (υ_x, 0, 0) states. It occurs at $\upsilon_x = 3$ for tetracene·He and at $\upsilon_x = 4$ for pentacene·He, precisely the states after which the levels of the x-mode progressions for the two complexes become evenly spaced; cf. Figure 6a. These states are energetically just above the corrugation features along the x axis, and thus the first whose wave functions can spread over the entire central region of the IPES.

C. Side-Crossing Delocalization of van der Waals Vibrational States. In the previous section, the focus was on the vdW states which, though extensively delocalized, are confined to one side of the molecular plane. However, at excitation energies above ∼30 cm^{-1} a growing number of side-crossing states appear in both complexes, which are significantly delocalized over both sides of the aromatic plane. One of the lowest-energy states of pentacene·He exhibiting such behavior is the y-mode state (0, 4, 0) at 28.83 cm^{-1}. Figure 10 displays the xy and yz cuts through its wave function; from the yz cut it is apparent that the wave function has appreciable amplitude in the $z = 0$ plane. This can be contrasted with the yz cut through the wave function of another y-mode state of pentacene·He, (0, 1, 0) in Figure 5, which shows the wave function completely localized on one side of the molecular plane.

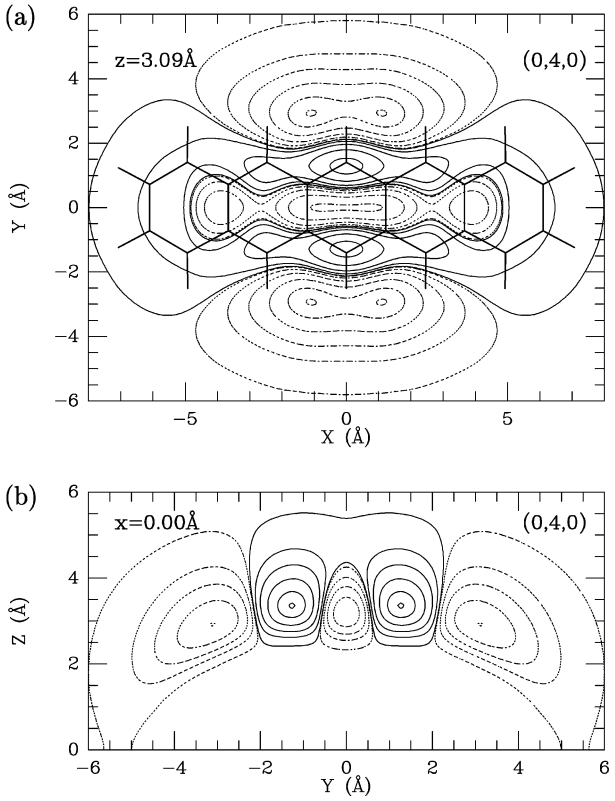

Figure 10. Cuts through the wave function of the vdW state (0, 4, 0) of pentacene·He in the *xy* (a) and the *yz* (b) planes. Contours are for 99, 80, 50, 25, 1, and 0.1% of the maximum amplitude for the respective cuts.

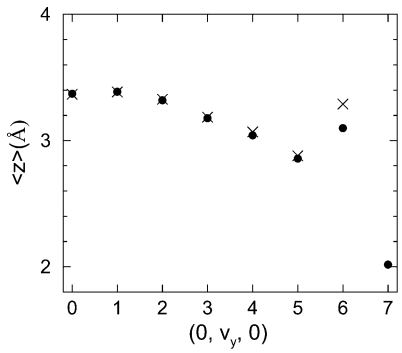

Figure 11. Expectation values $\langle z \rangle$ of the *z* coordinate, defined over the positive *z* range only, for the *y*-mode states (0, υ_y, 0) as a function of υ_y, for tetracene·He (●) and pentacene·He (×).

What the side-crossing states of tetracene·He and pentacene·He in Tables 4 and 5, respectively, have in common are large values of Δy and substantial Δz values, in combination with a low $\langle z \rangle$, a signature of the wave function amplitude shift from above and below the molecular plane to the peripheral regions around the aromatic molecule. The extent of the side-crossing delocalization is closely linked to the degree of excitation of the *y* mode, in the direction of the short molecular axis. This is conveyed by Figure 11, which shows a pronounced drop of $\langle z \rangle$ with increasing υ_y, for both vdW complexes. A notable deviation from this trend occurs for $\upsilon_y = 6$, when $\langle z \rangle$ conspicuously increases. The explanation is straightforward; the (0, 6, 0)? state is much less of a pure *y*-mode state than the other members of the (0, υ_y, 0) progression, due strong coupling to the *z* mode discussed in section IIIA. Consequently, the side-crossing delocalization is diminished and $\langle z \rangle$ rises.

Excitation of the *x* mode, along the long molecular axis, is much less effective in promoting the side-crossing delocalization, although the barriers in the *x* and *y* directions have similar heights. For energies at which excited *y*-mode states exhibit significant side-crossing delocalization, highly excited *x*-mode states are still largely localized on one side of the molecular plane. For example, the *y*-mode state (0, 7, 0)? of tetracene·He at 41.15 cm^{-1} has a low $\langle z \rangle$ of 2.02 Å, indicative of extensive side-crossing delocalization. In contrast, for the higher-energy *x*-mode state (10, 0, 0) at 41.96 cm^{-1}, $\langle z \rangle = 3.28$ Å, implying very little side crossing. Similarly, the *x*-mode state (9, 0, 0) of tetracene·He at 38.86 cm^{-1} has $\langle z \rangle = 3.37$ Å, suggesting complete confinement to one side of the molecule, whereas the *y*-mode state (0, 5, 0) at the significantly lower energy of 33.63 cm^{-1} has a much smaller $\langle z \rangle = 2.86$ Å, indicating considerable side crossing. The issue of mode dependence is addressed more thoroughly in the following section.

D. Energy Splittings and Their van der Waals Vibrational Mode Dependence. Another diagnostic criterion of the extent of side-crossing delocalization is the energy splitting between the pair of states that are symmetric/antisymmetric with respect to the aromatic plane; greater side-crossing delocalization gives rise to larger energy splittings. Beginning at ≈30 cm^{-1}, the energy splittings increase to ≥0.001 cm^{-1}, and they are listed in Tables 4 and 5. The largest energy splitting calculated for tetracene·He is 0.81 cm^{-1}, for state (0, 7, 0)?. In the case of pentacene·He, the largest identifiable splitting is 0.082 cm^{-1}, for state (0, 6, 0)?. The reason for such a big difference in the largest energy splittings is that for pentacene·He we were unable to identify unambiguously the symmetric and antisymmetric members of the *y*-mode (0, 7, 0) pair.

Closer examination of the data reveals strong vdW vibrational mode specificity of the energy splittings; at any given energy, the pair of states whose excitation energy is all, or primarily, in the *y* mode, has the energy splitting that is many times larger than that of the pair of states whose excitation is primarily in the *x* mode. Many instances of this can be found in Tables 4 and 5, but we highlight only a few. In Table 4, the already mentioned pair of *y*-mode states (0, 7, 0)? at 41.15 cm^{-1} has the energy splitting of 0.81 cm^{-1}, whereas the pair of *x*-mode states (10, 0, 0) at the higher energy of 41.96 cm^{-1} is split by much less, only 0.003 cm^{-1}. In Table 5, the energy splitting (0.004 cm^{-1}) of the pair of *x*-mode states (11, 0, 0)? at 38.45 cm^{-1} is 20 times smaller than the splitting (0.082 cm^{-1}) of the pair of *y*-mode states (0, 6, 0)? at 38.63 cm^{-1}. Perhaps even more strikingly, state (5, 3, 0), which is just 0.03 higher in energy, has an energy splitting that is 40 times smaller, 0.002 cm^{-1}. A similar degree of mode specificity of the energy splittings was found by us previously for S_1 2,3-DMN·He.[3] The much greater impact of the *y*-mode excitation on the size of the energy splittings, relative to that of the *x*-mode excitation, is due to (i) the shorter side-crossing path length along the *y* direction than in the *x* direction, and (ii) the smaller moment of inertia of the aromatic molecule, tetracene or pentacene, for the side-crossing motion in the *y* than in the *x* direction.[3] Of course, what makes the mode specificity possible in the first place is the overall weak coupling between the *x* and *y* modes in both vdW complexes. If these intermolecular vibrations were strongly coupled, the energy splittings would depend only on the total intermolecular energy, not on its distribution between the modes.

E. Connection with Experiment. Experimental information on the vdW vibrational excitations in the binary complexes of aromatic molecules with helium is generally scarce. To the best of our knowledge, only two vibronic bands have been observed

for S_1 tetracene·He, at 6.4 and 14.6 cm^{-1} to the blue of the electronic origin;[1] we are not aware of any such information for pentacene·He. Comparison with the vdW vibrational levels calculated for tetracene·He, shown in Table 4, suggests that the two observed bands could be tentatively assigned to the *x*-mode excitations (2, 0, 0) at 8.16 cm^{-1} and (4, 0, 0) at 16.07 cm^{-1}. Clearly, more experimental data are needed to verify this assignment, and to extend it to a larger set of excited states, which would also provide much needed experimental constraints for refining the IPESs.

It was mentioned in the Introduction that for tetracene embedded in liquid helium nanodroplets, the ZPL of the 0_0^0 band is split into two lines, designated α and β, which are separated by 1.1 cm^{-1}.[6-8] Hole-burning experiments have established that both the ground state S_0 and the electronically excited S_1 state are split into two levels, and that the two ZPLs originate from different ground states.[7] However, it has not been possible to determine experimentally the spacing of the two ground-state levels. The assumption that these two levels are in equilibrium with the helium bath has led to a rough estimate of the splitting in the S_0 ground state of ≤ 0.26 cm^{-1}, and about 1 cm^{-1} in the S_1 excited state.[7] The mechanism responsible for the splitting has not been determined. In one of several scenarios,[7] the splitting arises from the tunneling of one, or perhaps two, localized He atoms between the two equivalent global minima of the IPES, shown in Figure 2. However, the lowest vdW vibrational excitation calculated for S_1 tetracene·He is that of the *x*-mode (1, 0, 0) at 3.27 cm^{-1}. Even scaling it by 6.4/8.16, the ratio between the observed (tentatively) and the calculated (2, 0, 0) excitation, gives the value of 2.56 cm^{-1}, well above the estimated splitting of $\sim$1 cm^{-1} in the S_1 excited state. It is unlikely that the phenomenon of the ZPL splitting can be understood on the basis of the calculated vdW vibrational level structure of tetracene·He.

IV. Conclusions

We have reported a theoretical investigation of the quantum dynamics of the large-amplitude intermolecular vibrations of the van der Waals complexes tetracene·He and pentacene·He in the S_1 excited electronic state. Our study addressed the issues of the vdW vibrational level structure and mode coupling (wave function delocalization, side crossing, and associated energy splittings) on corrugated aromatic microsurfaces. Accurate quantum three-dimensional calculations of the coupled vdW vibrational levels of the two complexes were performed using the 3D DVR method.[17] This method gives numerically exact eigenvalues and eigenfunctions of the 3D intermolecular vibrational Hamiltonian,[23] which treats the large molecular as rigid.

The IPESs were modeled as a sum of atom−atom Lennard-Jones pair potentials, using the parametrization developed in our previous study of S_1 2,3-DMN·He vdW complex.[3] The IPES of tetracene·He has two equivalent minima 100.8 cm^{-1} deep on each side of the molecular plane, with the barrier between them 6.5 cm^{-1} high. The IPES of pentacene·He exhibits on each side of the pentacene moiety a central global minimum with the well depth of 102.9 cm^{-1} and two symmetrically equivalent secondary minima 101.3 cm^{-1} deep; the barrier height between the global and the secondary minima is 7.8 cm^{-1}, measured from the global minimum. In addition, the IPESs of tetracene·He and pentacene·He have two minor equivalent local minima further away from the center of the molecule, $\sim$11 and 13 cm^{-1}, respectively, above the global minimum. Thus the two IPESs exhibit corrugation along the long (*x*) axis of the aromatic molecule. But, relative to the well depths of 100−103 cm^{-1}, the corrugation of 11−13 cm^{-1} is relatively weak.

The vdW vibrational states of tetracene·He and pentacene·He analyzed in this work extend to 81 and 76%, respectively, of the well depths of the IPESs. The coupling between the long-axis (*x*) and short-axis (*y*) in-plane modes is weak, with a few exceptions, for the majority of states (υ_x, υ_y, 0) where the out-of-plane (*z*) mode is unexcited. In the pure *x*-mode (υ_x, 0, 0) and *y*-mode (0, υ_y, 0) progressions, the neighboring levels are evenly separated over a wide range of quantum numbers. The corrugation of the IPESs in the direction of the *x* axis perturbs only the low-lying *x*-mode states with excitation energies less than 12 cm^{-1}, up to $\upsilon_x = 3$ and 4 for tetracene·He and pentacene·He, respectively. In the energy range of the *z*-mode fundamental, 37−40 cm^{-1}, the coupling between the *y* and *z* modes is very strong, so that the state corresponding to the pure *z*-mode excitation could not be identified.

Spatial delocalization of the He atom parallel to the tetracene and pentacene plane is large already in the ground vdW state, with Δx equal to 1.14 and 1.34 Å for tetracene·He and pentacene·He, respectively. This stands in contrast with the near complete localization of one He atom in each of the two equivalent global minima above and below the benzene plane, observed in the PIMC calculations of benzene·He_{39}.[14] We believe that the difference is due to the much smaller microsurface provided by benzene compared to those of the larger polyaromatics, and to their corrugation, which is too weak to localize the He atom. Moreover, wave function delocalization parallel to the microsurfaces of tetracene and pentacene grows rapidly with the excitation of the in-plane *x* and *y* vibrational modes, with Δx and Δy increasing up to $\sim$5 and 4 Å, respectively. At the excitation energies of $\sim$40 cm^{-1}, spatial delocalization extends practically over the whole microsurface and is limited only by the finite size of the aromatic substrate. Delocalization perpendicular to the molecular plane measured by Δz, although substantial (0.3−1.1 Å), for most states is at least 2−3 times smaller than Δx and Δy.

At excitation energies >30 cm^{-1}, side-crossing delocalization of the wave function on both sides of the molecular plane begins to take place. This results in the energy splittings of the pairs of states which are symmetric/antisymmetric with respect to the aromatic plane. The largest identifiable energy splittings calculated in this work are 0.81 cm^{-1} for tetracene·He and 0.08 cm^{-1} for pentacene·He. The energy splittings show strong vdW vibrational mode specificity. At any particular energy, excitation of the *y* mode leads to energy splittings many times greater than if the *x* mode is excited. This is attributed to (a) the shorter side-crossing path length along the *y* direction than in the *x* direction, and (b) the smaller moment of inertia of the aromatic molecule around the *y* axis.

Our hope is that this study will motivate experimentalists to obtain spectroscopic data regarding the excited vdW vibrational states of tetracene·He and pentacene·He. This is crucial for the refinement of the IPESs of the two complexes, through the interplay between rigorous theory and experiments.

Acknowledgment. Z.B. is grateful to the National Science Foundation for partial support of this research, through Grant CHE-0315508. The computational resources used in this work were funded in part by the NSF MRI grant CHE-0420870.

References and Notes

(1) Even, U.; Al-Hroub, I.; Jortner, J. *J. Chem. Phys.* **2001**, *115*, 2069.
(2) Even, U.; Jortner, J.; Noy, D.; Lavie, N.; Cossart-Magos, C. *J. Chem. Phys.* **2000**, *112*, 8068.

(3) Bach, A.; Leutwyler, S.; Sabo D.; Bačić, Z. *J. Chem. Phys.* **1997**, *107*, 8781.
(4) Stienkemeier, F.; Vilesov, A. F. *J. Chem. Phys*. **2001**, *115*, 10119.
(5) Krasnokutski, S.; Rouillé, G.; Huisken, F. *Chem. Phys. Lett*. **2005**, *406*, 386.
(6) Hartmann, M.; Lindinger, A.; Toennies, J. P.; Vilesov, A. F. *Chem. Phys.* **1998**, *239*, 139.
(7) Hartmann, M.; Lindinger, A.; Toennies, J. P.; Vilesov, A. F. *J. Phys. Chem. A* **2001**, *105*, 6369.
(8) Hartmann, M.; Lindinger, A.; Toennies, J. P.; Vilesov, A. F. *Phys. Chem. Chem. Phys.* **2002**, *4*, 4839.
(9) Lehnig, R.; Slenczka, A. *J. Chem. Phys*. **2005**, *122*, 244317.
(10) Lehnig, R.; Slenczka, A. *Chem. Phys. Chem.* **2004,** *5*, 1014.
(11) Heidenreich, A.; Even, U.; Jortner, J. *J. Chem. Phys*. **2001**, *115*, 10175.
(12) Heidenreich, A. Jortner, J. *J. Chem. Phys*. **2003**, *118*, 10101.
(13) Felker, P. M.; Neuhauser, D. *J. Chem. Phys.* **2003**, *119*, 5558.
(14) Kwon, Y.; Whaley, K. B. *J. Chem. Phys.* **2001**, *114*, 3163.
(15) Whitley, H. D.; Huang, P.; Kwon, Y.; Whaley, K. B. *J. Chem. Phys.* **2005**, *123*, 054307.
(16) Huang, P.; Whitley, H. D.; Whaley, K. B. *J. Low Temp. Phys*. **2004**, *134*, 263.
(17) Mandziuk, M.; Bačić, Z. *J. Chem. Phys*. **1993**, *98*, 7165.
(18) Mandziuk, M.; Bačić, Z.; Droz, T.; Leutwyler, S. *J. Chem. Phys.* **1994**, *100*, 52.
(19) Droz, T.; Leutwyler, S.; Mandziuk, M.; Bačić, Z. *J. Chem. Phys*. **1994**, *101*, 6412.
(20) Droz, T.; Leutwyler, S.; Mandziuk, M.; Bačić, Z. *J. Chem. Phys.* **1995**, *102*, 4715.
(21) Droz, T.; Leutwyler, S.; Mandziuk, M.; Bačić, Z. *J. Chem. Phys*. **1995**, *103*, 4855.
(22) Mandziuk, M.; Bačić, Z. *J. Chem. Phys*. **1994**, *101*, 2126.
(23) Brocks, G.; van Koeven, D. *Mol. Phys*. **1988**, *63*, 999.
(24) Bačić, Z.; Light, J. C. *Annu. Rev. Phys. Chem*. **1989**, *40*, 469.
(25) Bačić, Z. Bound states of strongly coupled multidimensional molecular Hamiltonians by the discrete variable representation approach. In *Domain-Based Parallelism and Problem Decomposition Methods in Computational Science and Engineering*; Keyes, D. E., Saad, Y., Truhlar, D. G., Eds.; SIAM: Philadelphia, 1995; p 263.
(26) Liu, S.; Bačić, Z.; Moskowitz, J. W.; Schmidt, K. E. *J. Chem. Phys.* **1994**, *101*, 10181.
(27) Liu, S.; Bačić, Z.; Moskowitz, J. W.; Schmidt, K. E. *J. Chem. Phys*. **1995**, *103*, 1829.
(28) Sabo, D.; Bačić, Z.; Bürgi, T.; Leutwyler, S. *Chem. Phys. Lett*. **1995**, *244*, 283.
(29) Sabo, D.; Bačić, Z.; Graf, S.; Leutwyler, S. *J. Chem. Phys.* **1999**, *110*, 5745.
(30) Sabo, D.; Bačić, Z.; Graf, S.; Leutwyler, S. *J. Chem. Phys.* **1999**, *111*, 10727.
(31) Sabo, D.; Bačić, Z.; Graf, S.; Leutwyler, S. *J. Chem. Phys.* **1998,** *109*, 5404.
(32) Bahel, A.; Bačić, Z. *J. Chem. Phys*. **1999**, *111*, 11164.
(33) Xu, M.; Elmatad, Y.; Sebastianelli, F.; Moskowitz, J. W.; Bačić, Z. *J. Phys. Chem. B* **2006**, *110*, 24806.
(34) Sebastianelli, F.; Xu, M.; Elmatad, Y.; Moskowitz, J. W.; Bačić, Z. *J. Phys. Chem. C* **2007,** *111*, 2497.
(35) Bačić, Z.; Light, J. C. *J. Chem. Phys*. **1987**, *86*, 3065.
(36) Leutwyler, S.; Schmelzer, A.; Meyer, R. *J. Chem. Phys*. **1983**, *79*, 4385.